Supplementary Information for
A Solution-Gated Graphene FET Receiver for Molecular Communications with Low-Frequency PSD and Derivative-Based Detection

1 CAD-Based design of the MC Receiver

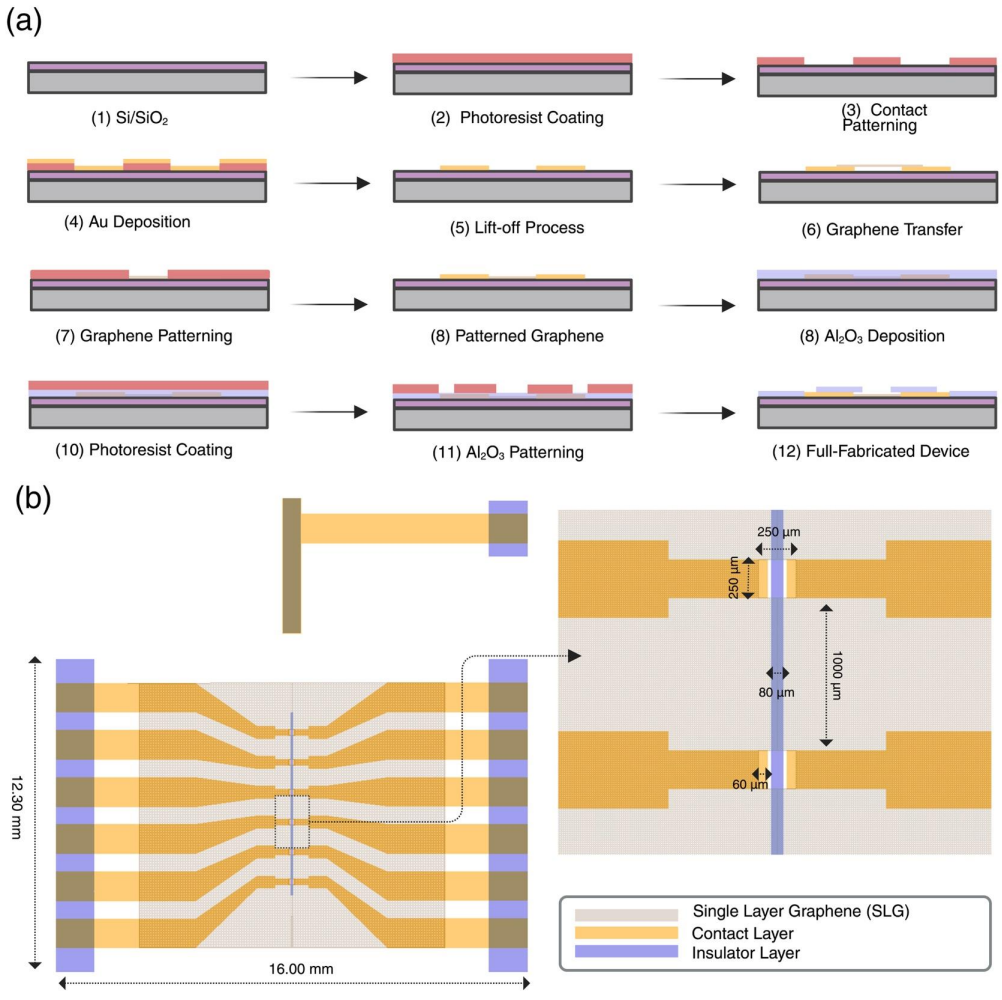

Figure S1. GFET fabrication process and device layout. (a) Process flow for the solution-gated GFET receiver. The fabrication sequence illustrates the patterning of Au electrodes on a Si/SiO_2 substrate, transfer and patterning of CVD graphene, and Al_2O_3 passivation with subsequent etching to define the active sensing window. (b) Device layout schematics illustrating the overall chip, the GFET sensing area, and the layered composition, with key dimensions indicated.

2 Characterization of the MC Receiver

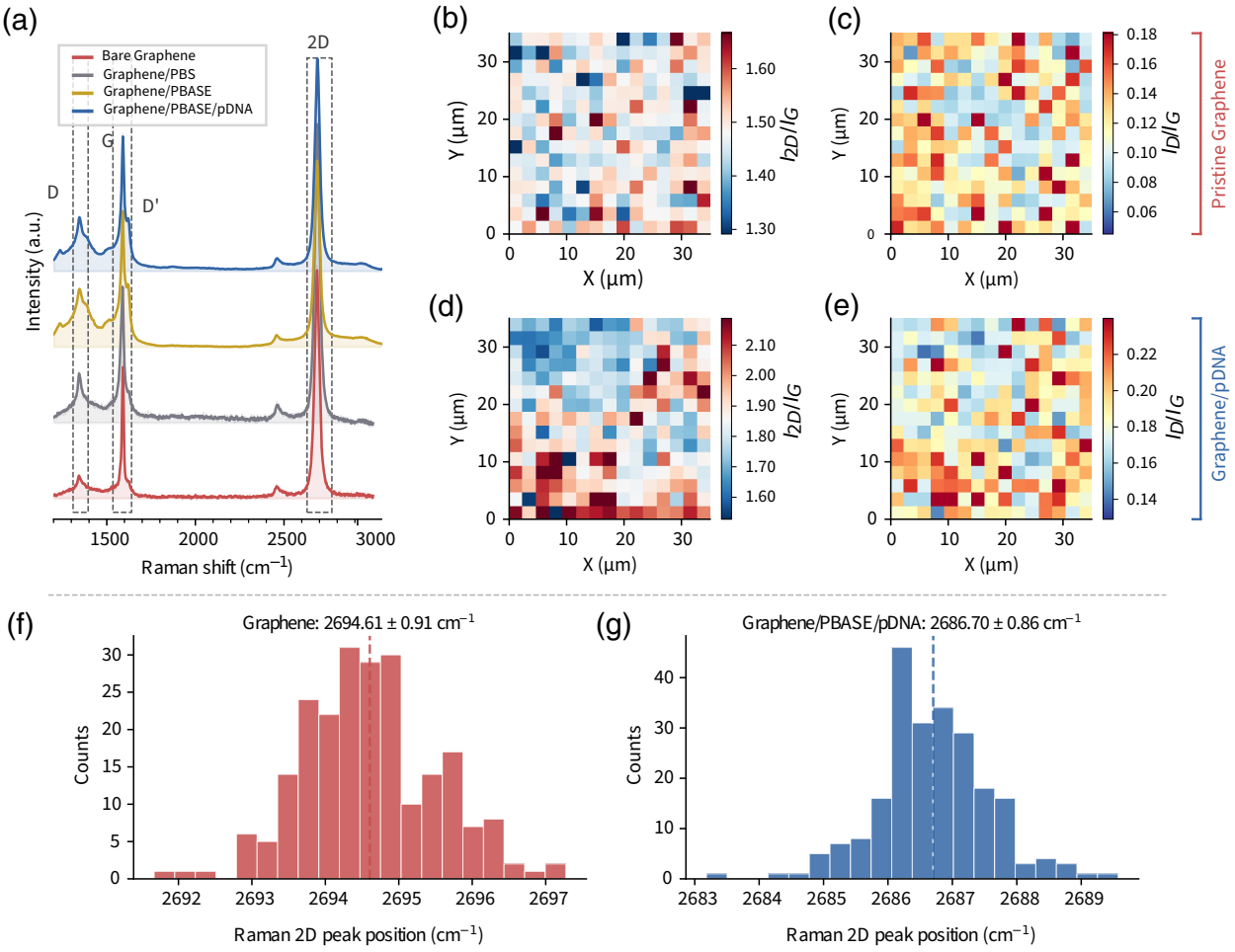

Figure S2. Raman spectroscopy analysis of the graphene surface during biofunctionalization. (a) Averaged Raman spectra collected at successive stages: pristine graphene, after PBS exposure, PBASE modification, and probe DNA (pDNA) immobilization. (b, c) Histograms comparing the 2D peak positions of (b) pristine graphene and (c) pDNA-functionalized graphene, indicating a redshift upon immobilization. (d-g) Spatial Raman intensity maps. (d) I_{2D}/I_G ratio and (e) I_D/I_G ratio of pristine graphene. (f) I_{2D}/I_G ratio and (g) I_D/I_G ratio after pDNA immobilization, confirming homogeneous functionalization with minimal induced defects.

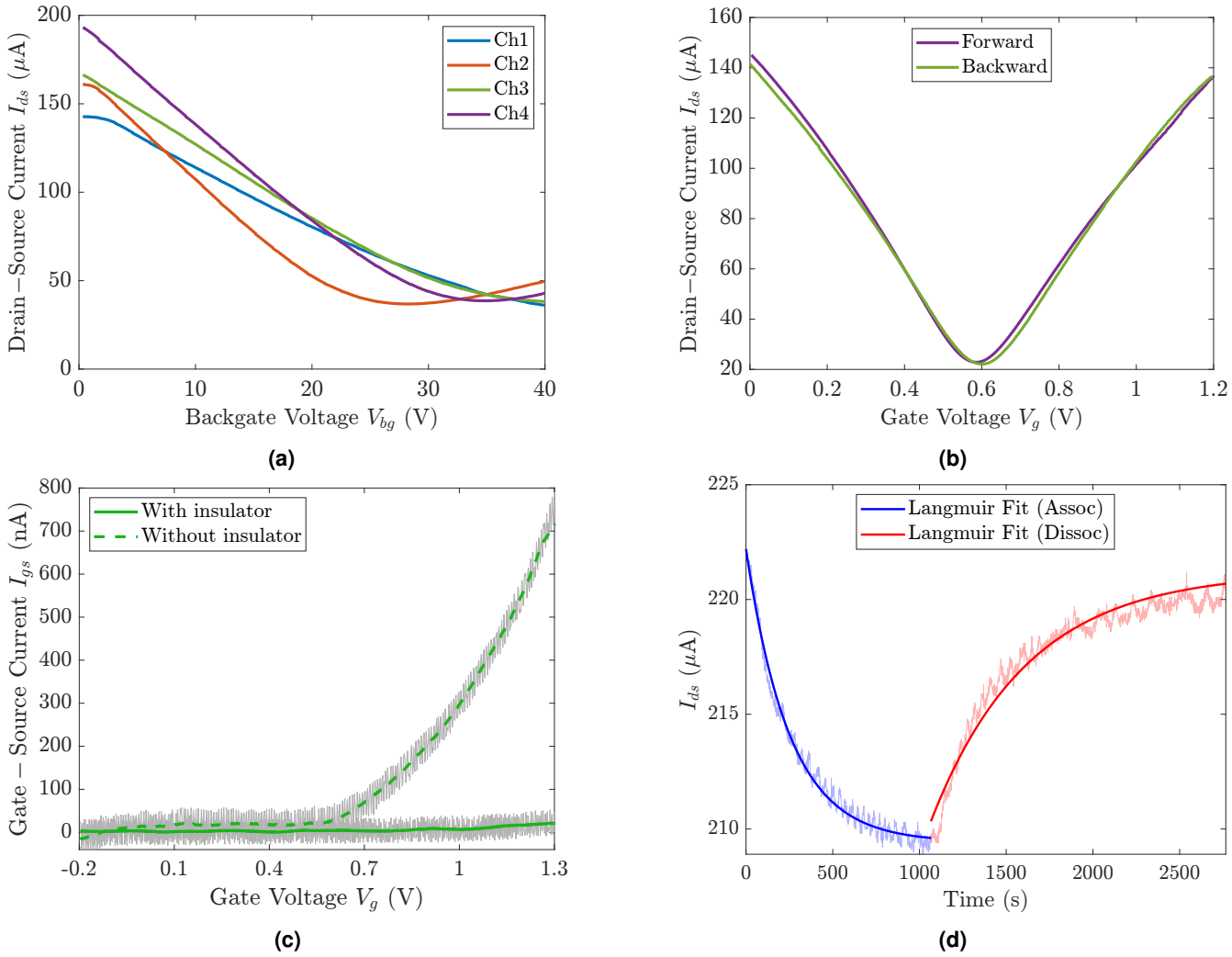

Figure S3. Electrical characterization of the GFET-based MC receiver. (a) Back-gate transfer characteristics (I_{ds} vs. V_{bg}) of four representative GFET channels used for extracting carrier mobility. (b) Solution-gate transfer characteristics (I_{ds} vs. V_g) showing negligible hysteresis. (c) Gate leakage current (I_{gs} vs. V_g) comparison between devices with and without the Al_2O_3 passivation layer. (d) Kinetic analysis of the association and dissociation phases, fitted to the Langmuir kinetic model (blue line for association, red line for dissociation).

3 Signal Detection Results Using Three Detection Methods

Scenario 1: Low Flow, Long Symbol Duration

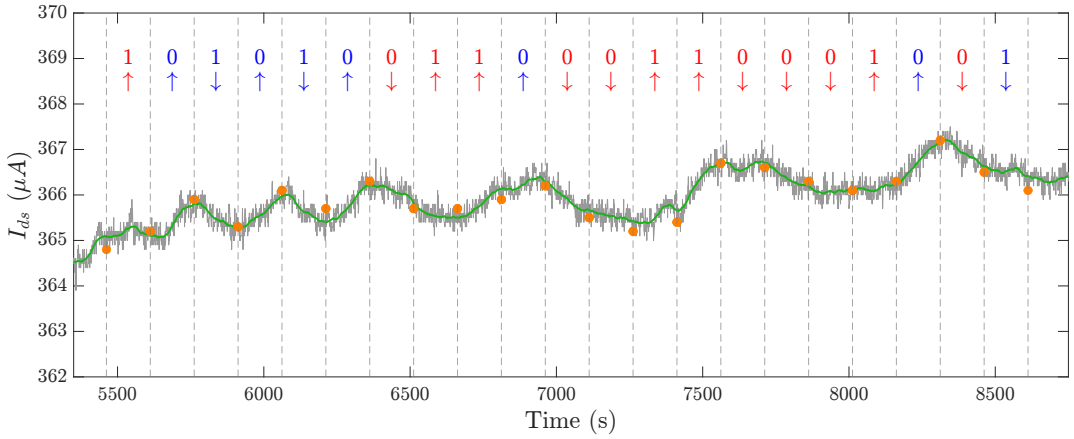

(a) Difference-based detection

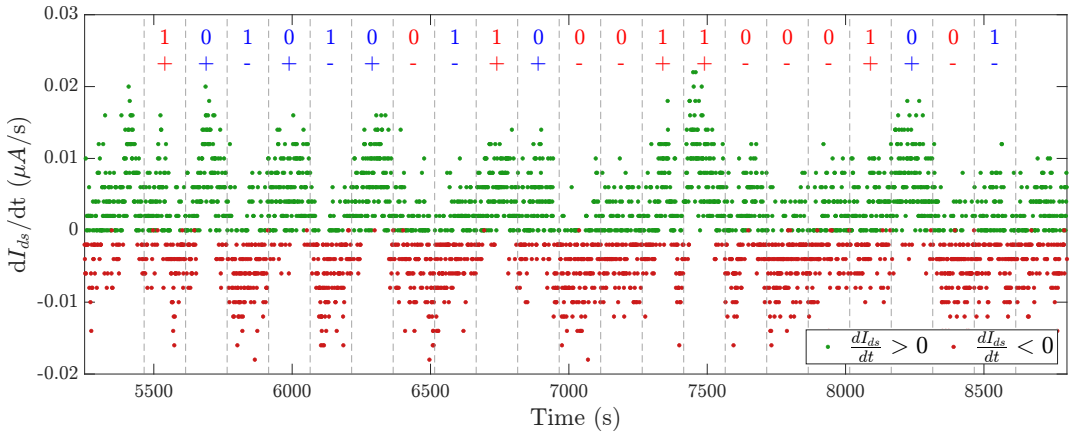

(b) Derivative-based detection

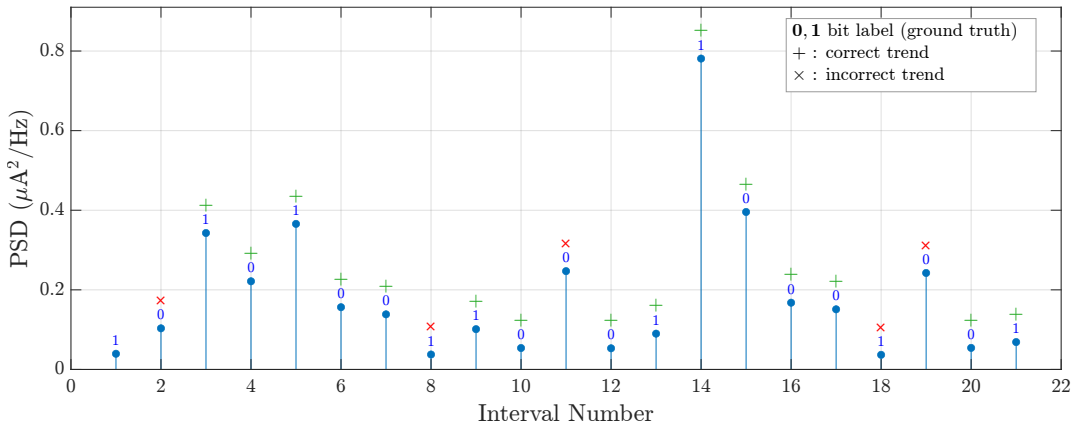

(c) Frequency-domain detection

Figure S4. Signal detection results for Scenario 1: Low Flow Rate, Long Symbol Duration ($T_p = 60\,s$, $T_s = 150\,s$, $u = 40\,\mu L/min$). The low flow rate results in weak signal modulation and significant drift (low SNR), leading to high BERs across all methods.

Scenario 2: High Flow rate, Short Symbol Duration

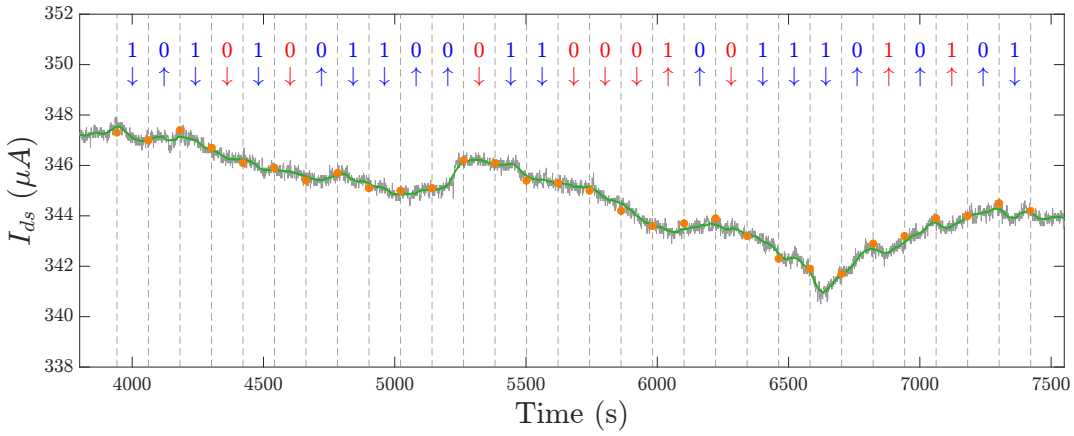

(a) Difference-based detection

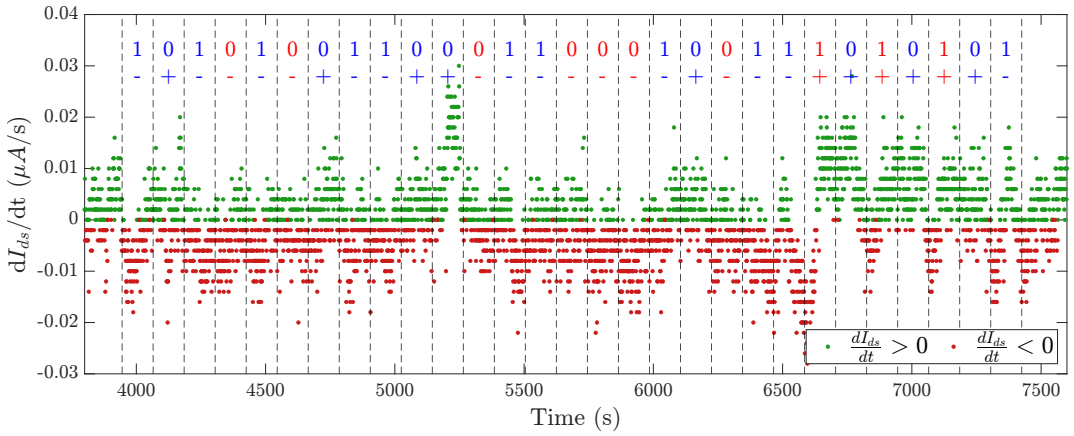

(b) Derivative-based detection

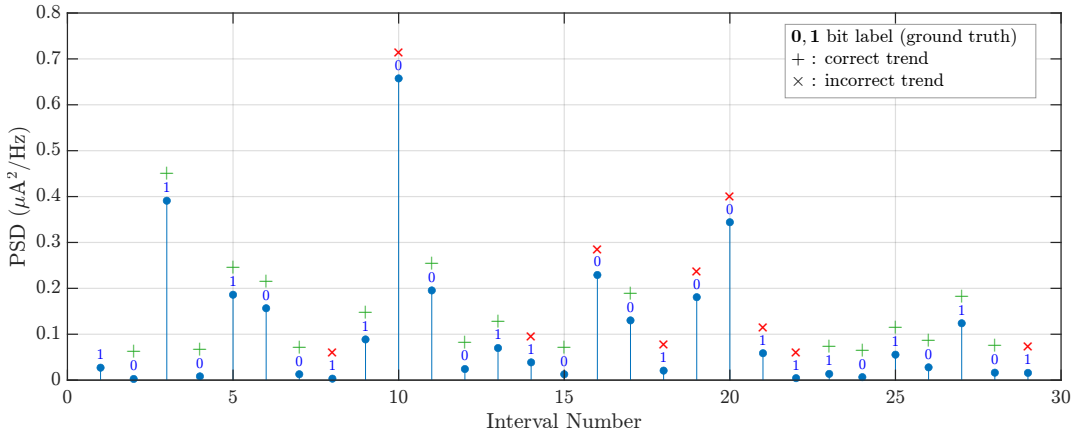

(c) Frequency-domain detection

Figure S5. High Flow Rate, Short Symbol Duration ($T_\mathrm{p} = 30\,\mathrm{s},\ T_\mathrm{s} = 120\,\mathrm{s},\ u = 80\,\mu\mathrm{L/min}$)

Scenario 3: Moderate Pulse Width, Short Symbol Duration

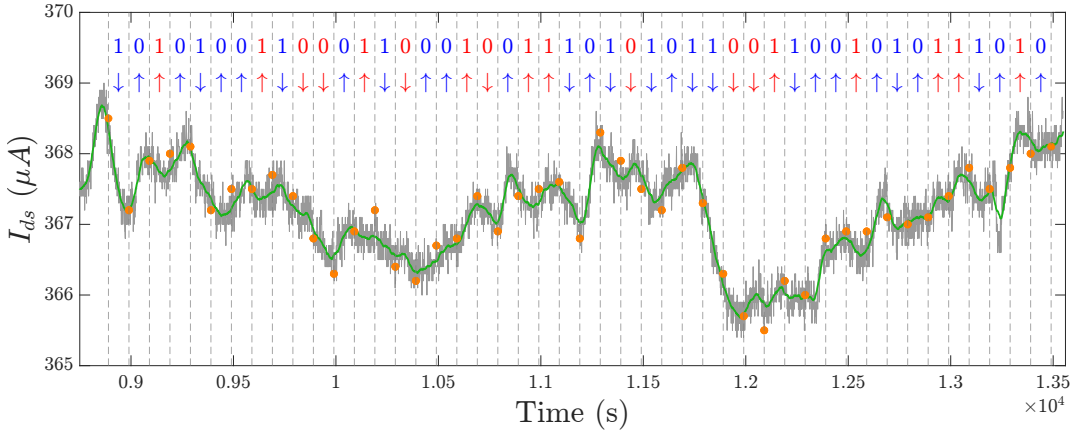

(a) Difference-based detection

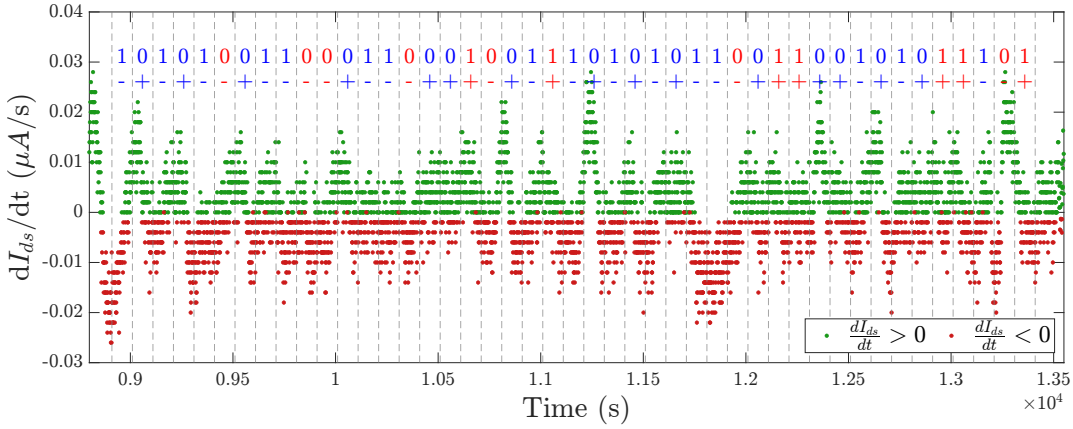

(b) Derivative-based detection

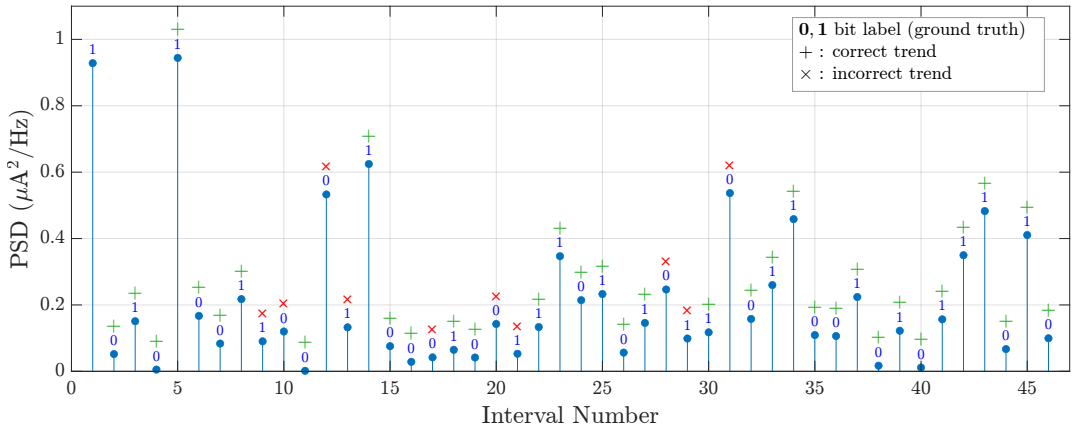

(c) Frequency-domain detection

Figure S6. Moderate Pulse Width, Short Symbol Duration ($T_\mathrm{p} = 40\,\mathrm{s},\ T_\mathrm{s} = 100\,\mathrm{s},\ u = 80\,\mu\mathrm{L/min}$).